Phospholamban structural dynamics in lipid bilayers probed by a spin label rigidly coupled to the peptide backbone

Christine B. Karim†, Tara L. Kirby, Zhiwen Zhang, Yuri Nesmelov, and David D. Thomas

Department of Biochemistry, Molecular Biology, and Biophysics, University of Minnesota, Minneapolis, MN 55455

Edited by David H. MacLennan, University of Toronto, Toronto, Canada, and approved August 9, 2004 (received for review April 22, 2004)

We have used chemical synthesis and electron paramagnetic resonance to probe the structural dynamics of phospholamban (PLB) in lipid bilayers. Derivatives of monomeric PLB were synthesized, each of which contained a single spin-labeled 2,2,6,6,-Tetramethylpiperidine-*N*-oxyl-4-amino-4-carboxylic acid amino acid, with the nitroxide-containing ring covalently and rigidly attached to the α-carbon, providing direct insight into the conformational dynamics of the peptide backbone. 2,2,6,6,-tetramethyl-piperidine-*N*-oxyl-4-amino-4-carboxylic acid was attached at positions 0, 11, and 24 in the cytoplasmic domain or at position 46 in the transmembrane domain. The electron paramagnetic resonance spectrum of the transmembrane domain site (position 46) indicates a single spectral component corresponding to strong immobilization of the probe, consistent with the presence of a stable and highly ordered transmembrane helix. In contrast, each of the three cytoplasmic domain probes has two clearly resolved spectral components (conformational states), one of which indicates nearly isotropic nanosecond dynamic disorder. For the probe at position 11, an N-terminal lipid anchor shifts the equilibrium toward the restricted component, whereas Mg^{2+} shifts it in the opposite direction. Relaxation enhancement, due to Ni^{2+} ions chelated to lipid headgroups, provides further information about the membrane topology of PLB, allowing us to confirm and refine a structural model based on previous NMR data. We conclude that the cytoplasmic domain of PLB is in a dynamic equilibrium between an ordered conformation, which is in direct contact with the membrane surface, and a dynamically disordered form, which is detached from the membrane and poised to interact with its regulatory target.

Muscle function depends critically on the active transport of calcium into the lumen of the sarcoplasmic reticulum (SR) by the Ca-ATPase, the SERCA gene product (1). SERCA activity is modulated in the heart by interaction with phospholamban (PLB), a 52-residue integral membrane protein (2–4). PLB inhibits SERCA at submicromolar calcium, but β-adrenergic stimulation causes phosphorylation of PLB at Ser-16 and/or Thr-17, relieving this inhibition (2, 5), activating calcium transport across the SR, and accelerating cardiac muscle relaxation (6–8). PLB is a major regulator of the dynamics of cardiac contractility (9, 10), and the SERCA–PLB calcium-regulatory system has been implicated in cardiovascular disease (11–13).

PLB is predominantly a homopentamer, with a small fraction of monomers, but it has been shown by electron paramagnetic resonance (EPR) (14, 15), fluorescence (16), and mutagenesis (17–19) that the less predominant monomeric form of PLB is primarily responsible for inhibition of SERCA. Therefore, the present study focuses on a stable PLB monomer, designated AFA-PLB, obtained by mutating the three Cys residues 36, 41, and 46 to Ala, Phe, and Ala, respectively (20–22). The isolated transmembrane domain of PLB inhibits SERCA just as effectively as does full-length PLB (3, 23, 24), whereas the isolated cytoplasmic domain has no effect on SERCA function (3, 21), nor do chimeric molecules in which the cytoplasmic domain is fused to another transmembrane sequence (25) or to a lipid anchor (21). Thus, the role of the cytoplasmic domain, upon phosphorylation or mutagenesis, is to modulate the inhibitory effects of the transmembrane domain (26).

The structural basis of the PLB–SERCA interaction has not been resolved. X-ray crystallography has produced structural models of SERCA with bound Ca^{2+} (27) and with bound thapsigargin (28), but there is no crystal structure of PLB. High-resolution structural models of monomeric PLB were first obtained from NMR in organic solvent (29, 30), but the most reliable current structural model of monomeric PLB is based on NMR of AFA-PLB in detergent micelles (22), depicted in Fig. 1. In the NMR-based model (22), two helical domains are connected by a five-residue (residues 17–21) semiflexible hinge, in an L-shaped configuration (Fig. 1). Solid-state NMR of AFA-PLB in oriented lipid bilayers showed that the C-terminal helix (cytoplasmic domain Ib, residues 22–29, and transmembrane domain II, residues 30–52) is approximately perpendicular to the membrane plane, with the cytoplasmic helix (residues 2–16) lying approximately along the bilayer surface (20) (Fig. 1).

EPR has become an important technique for investigating the structure and dynamics of membrane proteins. Site-directed spin labeling is typically accomplished by producing a single-Cys mutant of a protein and then labeling with a thiol-specific spin label. The EPR spectrum of a Cys-attached spin label is sensitive to tertiary and local dynamics at the labeled site, but the flexible attachment makes probe dynamics indirectly related to peptide backbone dynamics (31, 32). Pioneering work by Toniolo, Millhauser, and coworkers (33) has shown that the synthetic incorporation of 2,2,6,6,-tetramethyl-piperidine-*N*-oxyl-4-amino-4-carboxylic acid (TOAC), a spin-labeled amino acid (Fig. 1), provides a more compact probe that is rigidly coupled to the α-carbon and thus reports more accurately the position, orientation, and dynamics of the peptide backbone (34, 35). Therefore, we synthesized monomeric AFA-PLB with TOAC attached at position 0 (as an additional amino acid at the N terminus), at position 11 (in cytoplasmic domain Ia), at position 24 (in cytoplasmic domain Ib), and at position 46 (in transmembrane domain II) of the PLB sequence (Fig. 1). We co-reconstituted the labeled peptides in lipids, verified inhibitory function, and used EPR to determine the nanosecond rotational dynamics and membrane topology of these four labeled sites in lipid membranes. The results reveal features of the structural dynamics of PLB that are essential to understanding its regulatory function.

Materials and Methods

Synthesis of TOAC-Labeled PLB. Fig. 2 shows the sequence of the synthesized monomeric AFA-PLB peptides that incorporate the spin-labeled amino acid TOAC. PLB solid-phase peptide synthesis

This paper was submitted directly (Track II) to the PNAS office.

Abbreviations: EPR, electron paramagnetic resonance; PLB, phospholamban; SERCA, sarcoendoplasmic reticulum Ca-ATPase; TOAC, 2,2,6,6-tetramethyl-piperidine-*N*-oxyl-4-amino-4-carboxylic acid.

†To whom correspondence should be addressed. E-mail: cbk@ddt.biochem.umn.edu.

BIOPHYSICS

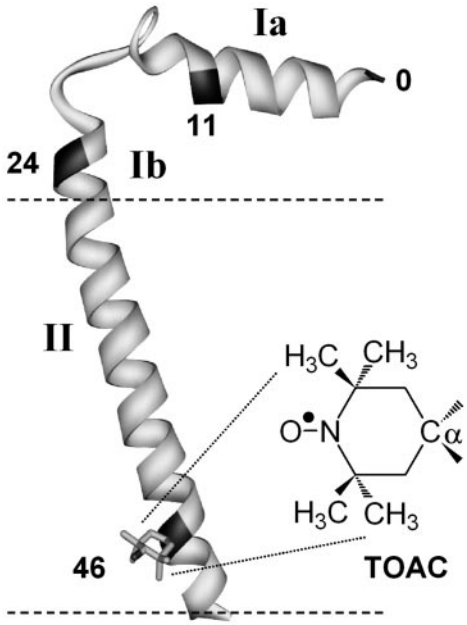

Fig. 1. Structural model of AFA-PLB, showing sites of TOAC spin labeling. Average structure was determined from NMR of AFA-PLB in detergent micelles (22). Dashed lines show approximate membrane surfaces.

was carried out essentially as described previously (21, 23, 36), except that 9-fluorenylmethyloxycarbonyl (Fmoc)-TOAC, synthesized as reported previously (33, 37), was incorporated at the N terminus (position 0) and at positions 11, 24, and 46 of the PLB sequence by manual coupling for 4 h using *N*-[(dimethylamino)-1*H*-1,2,3-triazolo[4,5-b]pyridin-1-ylmethylene]-*N*-methylmethanaminium hexafluorophosphate *N*-oxide (HATU)/*N,N*-diisopropylethylamine (DIEA) (1:2.4 eq) in *N*-methylpyrrolidone (NMP). At this point, a quantitative ninhydrin test was negative, confirming the quantitative coupling reaction. Deprotection and cleavage (38, 39) and regeneration of the nitroxide moiety (39, 40) were carried out as described previously. After preparative HPLC purification (36), fractions containing peptides were lyophilized to yield AFA-PLB (24.5%), 0-TOAC-AFA-PLB (14.8%), 11-TOAC-AFA-PLB (5.0%), 24-TOAC-AFA-PLB (6.9%), and 46-TOAC-AFA-PLB (3% yield based on starting resin). To obtain a derivative of spin-labeled PLB that has its N terminus anchored in the lipid bilayer, dialkyl 1′, 3′-dioctadecyl-*N*-succinyl-L-glutamate (lipid tail) was linked to 11-TOAC-AFA-PLB through the N-terminal amino group, as described previously for PLB residues 1–25 with a C-terminal Lys ($PLB_{1–25}K$) peptide amphiphile (21).

Peptide Analysis. We used a combination of analytical methods to identify and characterize the peptides. Mass spectrometry [matrix-assisted laser desorption/ionization time-of-flight (MALDI-TOF)], Edman protein sequencing, amino acid analysis, CD (21), inhibitory function (23), and EPR spectroscopy were carried out. Together, these methods established the high purity of the designed TOAC-labeled peptides.

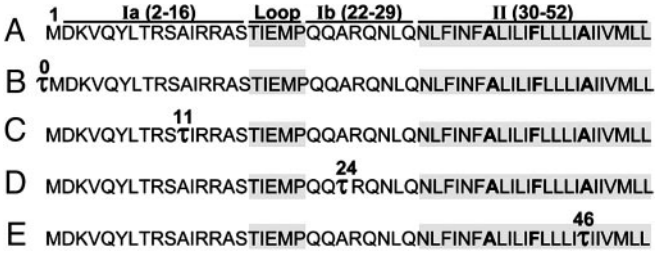

Fig. 2. Amino acid sequence of AFA-PLB (*A*), 0-TOAC-AFA-PLB (*B*), 11-TOAC-AFA-PLB (*C*), 24-TOAC-AFA-PLB (*D*), and 46-TOAC-AFA-PLB (*E*). The four proposed domains are indicated by shading. τ, TOAC.

Functional Analysis of Synthetic PLB Derivatives. Each PLB derivative was co-reconstituted in lipid bilayer membranes [dioleoylphosphatidylcholine (DOPC)/dioleoylphosphatidylethanolamine (DOPE), molar ratio 4:1] with purified SERCA at molar ratios of 10 PLB/SERCA and 700 lipids/SERCA (41, 42), and the calcium-dependence of ATPase activity was measured at 25°C as described previously (36). The data were plotted (V vs. pCa) and fit by the Hill equation

$$V = V_{max}/[1 + 10^{n\,(pK_{Ca}-pCa)}]\,, \qquad [1]$$

where V is the initial ATPase rate and n is the Hill coefficient. The data were normalized to the maximal rate, V_{max}, which was obtained from the fit, and then replotted to determine the shift in pK_{Ca} (pCa value required for 50% activation, where pCa = $-\log_{10}[Ca^{2+}]$, and K_{Ca} is the apparent Ca^{2+} dissociation constant).

EPR Spectroscopy. For EPR experiments, PLB was reconstituted into lipid vesicles containing DOPC/DOPE (4:1, 200 lipids per PLB) in 25 mM imidazole (pH 7.0) (43). It was found that doubling the ratio of lipids to PLB resulted in no change in EPR spectra, indicating that the conditions chosen are sufficient to avoid crowding artifacts (43). To measure accessibility to collision with Ni^{2+} ions localized to the lipid surface, DOGS-NTA or DOGS-NTA-Ni(II) (Avanti Polar Lipids) was substituted for 5 mole % of the lipid (43). Spectra were acquired by using a Bruker (Billerica, MA) eleXsys E 500 spectrometer equipped with the SHQ cavity, at 100-kHz field modulation with a peak-to-peak amplitude of 3.0 G (43). Except for saturation experiments, all spectra were recorded at a microwave power sufficiently low to avoid saturation. A typical sample contained 5 μl of 0.5 mM PLB, loaded into a 0.6-mm-inside-diameter TPX capillary (Medical Advances, Milwaukee, WI), with a total sample length of ≈10 mm. Sample temperature was maintained at 4°C by using the Bruker temperature controller, with the sample cell inside a quartz dewar. Samples for saturation experiments were flushed with N_2 gas to remove oxygen.

Analysis of Spin-Label Rotational Dynamics. Simulations of EPR spectra and fits to experimental spectra were carried out by using the program NLSL (44), using the MOMD model, in which the membranes are randomly oriented and all detectable (submicrosecond) rotational motion occurs relative to the membrane. Experimental spectra were fit by simulated spectra containing one or two populations (spectral components). For each population, rotational motion was characterized by a single mode of motion, with a rotational correlation time τ_R and an order parameter S. Rigid-limit values for magnetic interaction tensors were determined from spectra obtained at −60°C, and isotropic values were obtained from the free spin label in solution at 25°C. For each component, the order parameter S, the correlation time τ_R, and the mole fraction of that population were determined from the best-fit simulation. The uncertainty for each parameter was estimated from the range of values obtained by (*i*) starting the fits from a wide range of initial values and (*ii*) fitting spectra obtained from several different samples. To obtain a more intuitive interpretation of the order parameter, the motion was modeled as a wobble-in-cone with an angular amplitude θ_c (half-cone angle) given by

$$\theta_c = \cos^{-1}[0.5(1 + 8\mathbf{S})^{1/2} - 0.5]\,. \qquad [2]$$

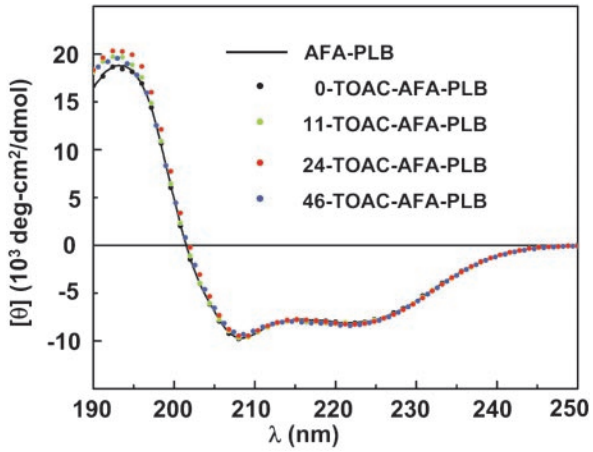

Fig. 3. CD spectra of AFA-PLB (—) and its TOAC derivatives in 10 mM Tris/0.2% octaethylene glycol monododecyl ether (C12E8), pH 7.0. CD spectra were recorded on a Jasco (Easton, MD) J-710 spectrophotometer at 25°C and analyzed as previously reported (21). Spectra are plotted as mean residue ellipticity, [θ].

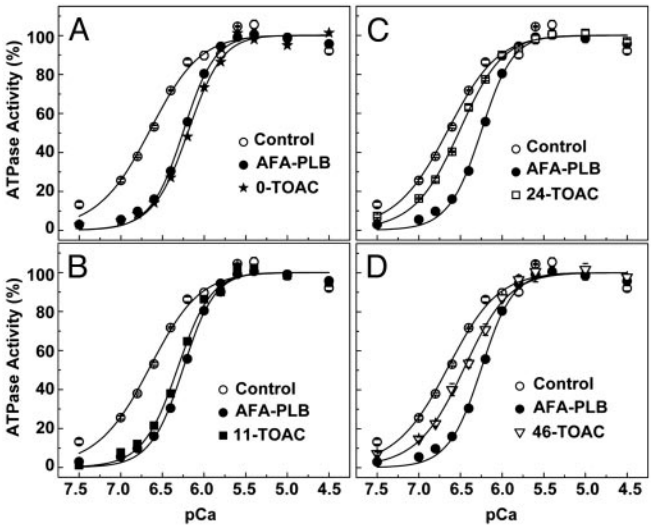

Fig. 4. Calcium-dependent ATPase activity at 25°C. The Ca-ATPase was reconstituted in the absence (○) and in the presence (●) of AFA-PLB alone and in the presence of AFA-PLB containing TOAC at positions 0 (⋆) (*A*), 11 (■) (*B*), 24 (□) (*C*), and 46 (▽) (*D*). Data sets were fit by Eq. **1** and plotted as V/V_{max}. Each point represents the mean ($n \geq 6$), and SEM was smaller than the plotted symbol.

The order parameter S is defined as the ensemble average of 1.5 $\cos^2\theta - 0.5$, where θ is the angular displacement that occurs during the EPR time window (10 ps to 1 μs).

Accessibility Analysis. Accessibility of the spin label to the membrane surface was determined from the decrease in EPR power saturation, caused by Ni^{2+} ions chelated to the lipid head-group [DOGS-NTA-Ni(II), Avanti Polar Lipids] (43, 45). The increase in the nitroxide relaxation rate, which is proportional to the frequency with which the spin label collides with the paramagnetic Ni^{2+} ions, is proportional to $\Delta P_{1/2}$, the increase in the microwave power level required to cause half-saturation (46). In this "saturation rollover" experiment, the signal intensity was recorded as a function of incident microwave power, and the data set was fit by

$$A = I * \sqrt{P}\,[1 + (2^{1/\varepsilon} - 1)P/P_{1/2}]^{-\varepsilon}, \qquad [3]$$

where A is the peak-to-peak amplitude of the central line in the EPR spectrum, P is the incident microwave power, $P_{1/2}$ is the microwave power at half-saturation, and ε depends on the inhomogeneity of the spectral line (46). In the nonlinear least-squares fit to Eq. **3** (ORIGIN 7.0, OriginLab, Northampton, MA), $P_{1/2}$ was allowed to vary freely and ε was allowed to vary between 0.5 and 1.5. Assuming that the only effect of the relaxant is to increase the spin-lattice relaxation rate, the collision frequency of the spin label with relaxant and, thus, the accessibility of the spin label to the lipid surface are proportional to $\Delta P_{1/2}$.

Results

Secondary Structures of AFA-PLB and TOAC-AFA-PLB. CD was used to determine whether the secondary structure of PLB was altered by TOAC incorporation into AFA-PLB. As shown in Fig. 3, the CD spectra for TOAC-AFA-PLB in octaethylene glycol monododecyl ether (C12E8) are virtually identical to that of AFA-PLB (Fig. 3) and to that of wild-type PLB (Figs. 10 and 11, which are published as supporting information on the PNAS web site), except at short wavelengths, where the variation is within experimental error caused by light scattering. Analysis of these spectra as linear combinations of basis spectra indicates 85–90% helical content, as previously reported for AFA-PLB (21). We conclude that the introduction of the TOAC amino acid into the PLB sequence has negligible effects on PLB secondary structure. It is often stated that TOAC, like the closely related α-aminoisobutyric acid, tends to increase the α-helical content of peptides (47, 48). However, the only direct spectroscopic demonstration of this effect in aqueous solution is for short (16- to 20-residue) peptides, each containing a pair of TOAC residues (49). Further work will be needed to determine whether single TOAC residues cause increases in α-helical content in PLB that are too small to be detected by CD. Although PLB is a highly helical peptide, we report below that the TOAC EPR spectrum resolves a small but significant population having a disordered peptide backbone conformation at three different positions in the cytoplasmic domain of PLB, showing that TOAC is capable of detecting deviations in helical order.

Inhibitory Function of AFA-PLB and TOAC-AFA-PLB Derivatives. The inhibition of Ca-ATPase activity was quantified by the shift in pK_{Ca} (the pCa value required for 50% activation). Consistent with our previous results (21), monomeric AFA-PLB induced a 4-fold increase in K_{Ca} (Fig. 4*A*), shifting pK_{Ca} from 6.66 ± 0.01 to 6.25 ± 0.01. This shift of 0.41 ± 0.02 is similar to the effect of wild-type PLB, described in *Supporting Materials and Methods*, which is published as supporting information on the PNAS web site. All four TOAC spin-labeled derivatives retained at least some inhibitory potency. Introduction of TOAC at position 0 (Fig. 4*A*) or 11 (Fig. 4*B*) had little or no effect. Introduction of TOAC reduced the pCa shift to 0.12 ± 0.02 at position 24 (Fig. 4*C*) and to 0.20 ± 0.02 at position 46 (Fig. 4*D*).

EPR Dynamics of TOAC Spin-Labeled PLB. The incorporation of TOAC into PLB allows us to detect directly the nanosecond peptide backbone dynamics in distinct domains of PLB. Fig. 5 shows the EPR spectra of four different TOAC-containing AFA-PLBs reconstituted in lipid bilayers. The spectra reveal dramatic differences in nanosecond rotational dynamics, from the narrow spectrum of the N-terminal probe in the cytoplasmic domain, indicating large-amplitude nanosecond rotational motion (dynamic disorder) (Fig. 5, trace 0), to the broad spectrum of the probe at position 46 in the transmembrane domain, indicating highly restricted motion (order) (Fig. 5, trace 46). Whereas the probe at position 46 shows only a single spectral component, suggesting a single well defined and ordered conformation, each of the three cytoplasmic domain probes shows two well resolved spectral components, both ordered and disordered, demonstrating two conformations of the peptide

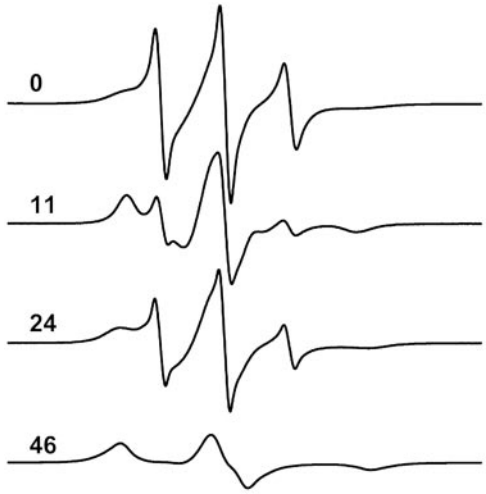

Fig. 5. EPR spectra of TOAC-labeled PLB, labeled at the indicated position (0, 11, 24, and 46) on AFA-PLB, incorporated into lipid bilayers. Spectra, obtained with a 120-G scan width at 4°C, were normalized to unit concentration by dividing by the double integral.

backbone. These results are consistent with a PLB structural model in which the transmembrane domain is a highly ordered helix, and the cytoplasmic domain is in a dynamic equilibrium between ordered and dynamically disordered forms.

Rotational dynamics was analyzed quantitatively as described in *Materials and Methods* and summarized in Table 1. At position 46, the rotational motion is highly restricted, as evidenced by the long correlation time (35 ns) and high order parameter (0.94, corresponding to a 16° amplitude). Each of the cytoplasmic domain probes also has a substantial ordered component, but the correlation time of this component is much shorter (5–7 ns), and the order parameter is substantially less, indicating a much larger angular amplitude. Each of the cytoplasmic domain probes has a dynamically disordered component, characterized by a subnanosecond correlation time and a very low order parameter, indicating essentially unrestricted motion. The mole fraction of this component (Table 1) is greatest at position 0 (46%) and least at position 11 (10%).

Modulation of the Dynamic Equilibrium in the Cytoplasmic Domain. The N-terminal lipid anchor almost completely eliminates the dynamically disordered population in 11-TOAC-AFA-PLB [Fig. 6, top trace (structure shown in Fig. 13, which is published as supporting information on the PNAS web site)], indicating that the ordered component corresponds to a conformation in which the cytoplasmic domain contacts the lipid surface. In contrast, 20 mM $MgCl_2$ increases the mole fraction of the disordered population

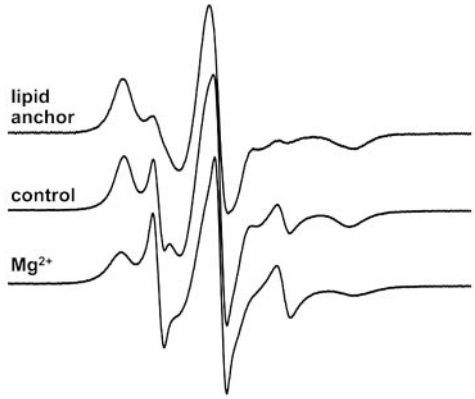

Fig. 6. EPR spectra of membranes containing 11-TOAC-AFA-PLB (middle trace), as affected by an N-terminal lipid anchor (top trace) or by 20 mM Mg^{2+} (bottom trace). Spectra were acquired and plotted as in Fig. 5, except that the vertical scale was expanded by a factor of 2.

(Fig. 6, bottom trace). When the ionic strength was increased to the same extent by adding 60 mM KCl instead of $MgCl_2$, there was no significant effect on the EPR spectrum (data not shown), indicating that the effect of Mg^{2+} is caused specifically by its binding (50). The simplest explanation, consistent with the effect of the lipid anchor, is that the cationic Mg^{2+} competes with the cationic PLB cytoplasmic domain for binding sites on the lipid surface, thus increasing the fraction of cytoplasmic domains that are detached from the membrane surface and, therefore, dynamically disordered.

Accessibility to the Membrane Surface. We used power saturation to measure the accessibility of the spin label to Ni^{2+} ions chelated to the lipid head-group. Fig. 7 shows that the highest accessibility was observed at position 0, was ≈30% less at position 11, and was another 40% less at position 24. TOAC at position 46 was completely inaccessible to the membrane surface. These results confirm that the transmembrane domain of PLB is deeply embedded in the membrane as indicated in Fig. 1 (22), but they suggest that the model shown in Fig. 1 should be modified slightly to show positions 0 and 11 interacting more with the lipid surface than does position 24 (see below).

Discussion

Advantages of TOAC. Previous studies used TOAC to probe the conformational dynamics of short peptides binding to membrane surfaces, including 11-residue lipopeptide antibiotics (34, 35) and six- or seven-residue basic peptides (51). The present study establishes TOAC as a powerful probe of structural dynamics of multidomain integral membrane proteins. Because TOAC is rigidly coupled to the peptide backbone, it reflects backbone dynamics directly (34, 51). This provides a substantial advantage over con-

Table 1. TOAC dynamics of AFA-PLB

	Ordered				Disordered		
Pos.	X	S	θ_c,°	τ_R, ns	S	θ_c,°	τ_R, ns
0	0.54 ± 0.09	<0.45	<0.05	5.9 ± 1.8	<0.05	≥90	0.38 ± 0.08
11	0.90 ± 0.03	0.71 ± 0.09	37 ± 7	5.3 ± 2.0	0.08 ± 0.03	82 ± 8	0.70 ± 0.30
24	0.70 ± 0.06	0.73 ± 0.09	36 ± 7	7.1 ± 2.2	<0.05	≥90	0.44 ± 0.12
46	1.00	0.94 ± 0.03	16 ± 4	35 ± 12			

Parameters were obtained from analysis of EPR spectra with NLSL as described in *Materials and Methods*. Uncertainties indicate the range of input values that gave acceptable fits; i.e., peak positions and relative line heights of the simulated spectrum were within experimental error of the observed spectrum. Best fits are illustrated in Fig. 12, which is published as supporting information on the PNAS web site. Pos., position; X, mole fraction; S, order parameter; θ_c, cone angle derived from *S* (Eq. **2**); τ_R, rotational correlation time.

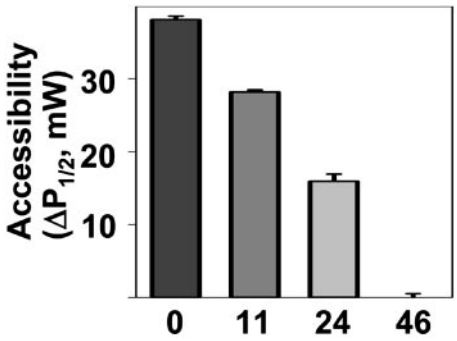

Fig. 7. Accessibility of TOAC, at the indicated position (0, 11, 24, and 46) in AFA-PLB, to the membrane surface. $\Delta P_{1/2}$ is the increase in $P_{1/2}$, determined from Eq. **3**, due to surface-bound Ni^{2+} ions.

ventional methods of site-directed spin labeling, in which the attachment of probes to Cys side chains leaves several flexible bonds between the α-carbon and the nitroxide group, thus leaving considerable ambiguity about the interpretations of spectra. In principle, the six-membered ring containing the nitroxide moiety in TOAC could have some conformational flexibility, but the high order parameter (0.94) observed for TOAC at position 46 establishes an upper bound of 16° (Table 1) for the amplitude of orientational fluctuations of the nitroxide group relative to the peptide backbone. Thus, with TOAC, the correlation times and order parameters determined from the spectra are reliable reflections of peptide backbone dynamics. The reduction in the probe's possible modes of motion allows us to clearly resolve distinct dynamic modes and to assign them to distinct conformations of the peptide backbone.

These points are illustrated by Fig. 8, which compares the spectrum of TOAC-labeled PLB with that of PLB labeled at the same position by the conventional Cys-directed method (43). The mobile components of the two spectra are comparable, but the other component is much more restricted for TOAC, resulting in greatly improved resolution. Similarly, measurements of distance or accessibility are more simply interpreted with TOAC, because the location of the nitroxide relative to the α-carbon is severely constrained. Another significant advantage of TOAC derivatives is that they can be synthesized routinely in large quantities, offering the opportunity to perform more extensive studies with a single preparation. However, TOAC is sensitive to oxidation and to acidic media, which is required for peptide synthesis. This makes an extensive labeling study much more time-consuming and expensive than when using the method involving Cys-scanning mutagenesis. Nevertheless, the models of molecular structure and dynamics

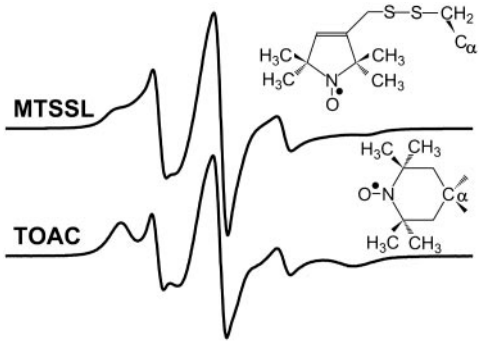

Fig. 8. EPR spectra in lipid bilayers of AFA-PLB labeled at position 11 with Cys-directed methanethiosulfonate spin label (MTSSL) (*Upper*) or TOAC (*Lower*). Spectra were acquired and plotted as in Fig. 5.

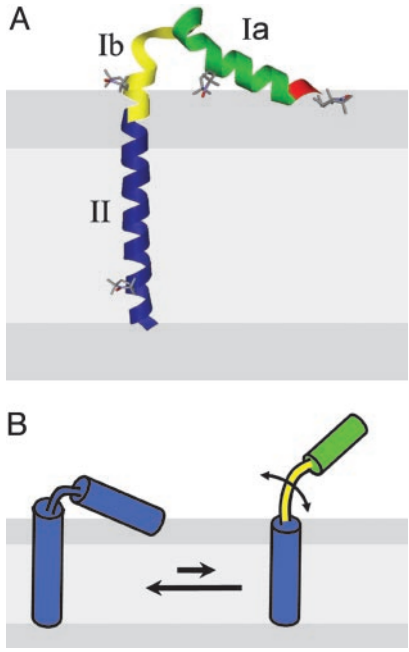

Fig. 9. Model of PLB topology and structural dynamics in the membrane, based on the NMR structure of AFA-PLB in detergent micelles (22) and on EPR of the four TOAC derivatives in the present study. Membrane head-group layers (10 Å thick) and the hydrocarbon layer (30 Å thick) are indicated schematically. (*A*) NMR solution structure of the ordered conformation, colored spectrally to indicate backbone dynamics, increasing from blue to green to yellow to red. (*B*) Two-state model supported by the EPR spectra (see Figs. 5 and 6), in which the ordered conformer (*Left*) is in dynamic equilibrium with a more dynamic conformer (*Right*).

derived from TOAC spectra are likely to be much more quantitatively accurate than those produced by conventional site-directed spin labeling.

Structural Dynamics of PLB. The principal conclusions of the present study are illustrated by Fig. 9. EPR spectra of TOAC-labeled PLB in membranes (Fig. 5 and Table 1) reveal that the peptide backbone of PLB is quite rigid in the transmembrane domain at position 46 (Fig. 5, trace 46, order parameter 0.94), as expected for a well ordered α-helix. However, the cytoplasmic domain is characterized by considerable nanosecond dynamics. It is not surprising that the N-terminal probe gives a spectrum indicating large-amplitude nanosecond dynamics (Fig. 5, trace 0, and Table 1), but it is remarkable that the probes at positions 11 and 24, which are in segments corresponding to well ordered α-helices in the NMR structure of AFA-PLB (22), also contain clear evidence for nanosecond dynamics. The probe at position 24 is more dynamic than the probe at position 11 (Fig. 5). Fig. 9*A* illustrates these results, based on the highly ordered NMR structure, with color used to illustrate dynamics, showing that domain Ib (yellow, residues 17–29) is more dynamic than domain Ia (green, residues 2–16). Although we only have EPR data from probes at four sites, the domain coloring in Fig. 9*A* is justified by the results of NMR relaxation studies in detergent micelles, which show that backbone dynamics is fairly uniform within each of these domains (52). The topology of this model, with residues 0 and 11 less solvent-exposed than residue 24, is based primarily on the relaxation enhancement studies (Fig. 7) showing that positions 0 and 11 are more accessible to the membrane surface than is position 24. This model is consistent with previous solution NMR results in micelles (22) and solid-state NMR results in lipid bilayers (20).

Fig. 9*A* accurately reflects the conclusions of the present study in

the context of the NMR structural model of PLB, but it fails to depict the most striking feature of the EPR data: the observation of two well resolved conformational states in the cytoplasmic domain (43), as detected by TOAC probes at positions 11 and 24 (Fig. 5). In both cases, the major population has a broad spectrum that is consistent with a moderately stable α-helix, but a significant fraction has a sharp spectrum indicating nearly isotropic nanosecond disorder. This spectral component, characterized by an order parameter <0.1 (Table 1), implies a degree of dynamic disorder that is much too great to represent an ordered α-helix and must, therefore, correspond to at least a partially unfolded structure (53). Fig. 9*B* illustrates the conclusion that there are two conformations present in the cytoplasmic domain, an ordered conformation that is well represented by the NMR structure (Fig. 9*B Left*) and a second conformation (Fig. 9*B Right*) in which a substantial portion of the cytoplasmic domain, extending well beyond both ends of the "hinge" (residues 17–21), is dynamically disordered. Fig. 6 shows that the dynamic equilibrium between these two structural states of PLB is quite sensitive to environmental conditions and that the ordered conformation is stabilized by interaction with the membrane surface, as illustrated in Fig. 9*B*.

The present study illustrates the complementary nature of two techniques, ^{15}N-NMR and TOAC EPR, for investigating peptide backbone dynamics. The principal advantage of NMR is that it provides information about all amino acids in the protein in a single sample, but high-resolution NMR requires the use of rapidly tumbling micelles, with nanosecond correlation times and zero order parameters, eliminating the capability to resolve ordered and disordered conformations. EPR has the sensitivity to detect these motions in lipid bilayers and to resolve the ordered and disordered conformational states. Although NMR does not resolve the two conformational states directly, NMR relaxation studies have shown evidence for an exchange process in the cytoplasmic domain of PLB in the micro- to millisecond time range that is consistent with the EPR data (52).

We propose that this conformational equilibrium is crucial to the function of PLB and is regulated by phosphorylation and by PLB's interactions with SERCA and cAMP-dependent protein kinase (PKA). In support of this concept, a recent EPR study of a spin label attached to Cys at position 11 confirms that this site on PLB interacts strongly with the membrane surface in the absence of SERCA and that SERCA causes a major conformational shift in PLB, causing the cytoplasmic domain to be raised substantially above the membrane surface (43). Further studies of TOAC-labeled PLB in membranes containing SERCA and/or PKA are needed to provide a more complete picture of this dynamic membrane-embedded regulatory system.

We thank Germana Paterlini (Certusoft, Inc., Minneapolis) for assistance with molecular modeling and graphics; Razvan Cornea, Gianluigi Veglia, and Jamillah Zamoon for helpful discussions; Nathan Lockwood (Department of Chemical Engineering and Materials Science, University of Minnesota) for providing the lipid anchor; Florentin Nitu for technical assistance; Thomas Krick for assistance with mass spectrometry; Joseph McNulty and Glenn Millhauser (University of California, Santa Cruz) for advice on TOAC synthesis; Jinny Johnson and Lawrence Dangott (Protein Chemistry Laboratory, Texas A&M University, College Station) for amino acid analysis; and Henriette Remmer (Protein Structure Facility, University of Michigan, Ann Arbor) for helpful discussions. This work was supported in part by American Heart Association Grant 9930083N (to C.B.K.) and National Institutes of Health Grant GM27906 (to D.D.T.).

1. MacLennan, D. H., Rice, W. J. & Odermatt, A. (1997) *Ann. N. Y. Acad. Sci.* **834,** 175–185.
2. Simmerman, H. K. & Jones, L. R. (1998) *Physiol. Rev.* **78,** 921–947.
3. Reddy, L. G., Jones, L. R., Cala, S. E., O'Brian, J. J., Tatulian, S. A. & Stokes, D. L. (1995) *J. Biol. Chem.* **270,** 9390–9397.
4. Toyofuku, T., Kurzydlowski, K., Tada, M. & MacLennan, D. H. (1994) *J. Biol. Chem.* **269,** 22929–22932.
5. Colyer, J. (1993) *Cardiovasc. Res.* **27,** 1766–1771.
6. Stokes, D. L. (1997) *Curr. Opin. Struct. Biol.* **7,** 550–556.
7. Sasaki, T., Inui, M., Kimura, Y. & Tada, M. (1992) *J. Biol. Chem.* **267,** 1674–1679.
8. Lindemann, J. P., Jones, L. R., Hathaway, D. R., Henry, B. G. & Watanabe, A. M. (1983) *J. Biol. Chem.* **258,** 464–471.
9. Haghighi, K., Schmidt, A. G., Hoit, B. D., Brittsan, A. G., Yatani, A., Lester, J. W., Zhai, J., Kimura, Y., Dorn, G. W., II, MacLennan, D. H. & Kranias, E. G. (2001) *J. Biol. Chem.* **276,** 24145–24152.
10. Zhai, J., Schmidt, A. G., Hoit, B. D., Kimura, Y., MacLennan, D. H. & Kranias, E. G. (2000) *J. Biol. Chem.* **275,** 10538–10544.
11. MacLennan, D. H. & Kranias, E. G. (2003) *Nat. Rev. Mol. Cell Biol.* **4,** 566–577.
12. Schmidt, A. G., Edes, I. & Kranias, E. G. (2001) *Cardiovasc. Drugs Ther.* **15,** 387–396.
13. Minamisawa, S., Hoshijima, M., Chu, G., Ward, C. A., Frank, K., Gu, Y., Martone, M. E., Wang, Y., Ross, J., Jr., Kranias, E. G., Giles, W. R. & Chien, K. R. (1999) *Cell* **99,** 313–322.
14. Thomas, D. D., Reddy, L. G., Karim, C. B., Li, M., Cornea, R., Autry, J. M., Jones, L. R. & Stamm, J. (1998) *Ann. N. Y. Acad. Sci.* **853,** 186–194.
15. Cornea, R. L., Jones, L. R., Autry, J. M. & Thomas, D. D. (1997) *Biochemistry* **36,** 2960–2967.
16. Li, M., Reddy, L. G., Bennett, R., Silva, N. D., Jr., Jones, L. R. & Thomas, D. D. (1999) *Biophys. J.* **76,** 2587–2599.
17. Reddy, L. G., Jones, L. R. & Thomas, D. D. (1999) *Biochemistry* **38,** 3954–3962.
18. Autry, J. M. & Jones, L. R. (1997) *J. Biol. Chem.* **272,** 15872–15880.
19. Kimura, Y., Kurzydlowski, K., Tada, M. & MacLennan, D. H. (1997) *J. Biol. Chem.* **272,** 15061–15064.
20. Mascioni, A., Karim, C., Zamoon, J., Thomas, D. D. & Veglia, G. (2002) *J. Am. Chem. Soc.* **124,** 9392–9393.
21. Lockwood, N. A., Tu, R. S., Zhang, Z., Tirrell, M. V., Thomas, D. D. & Karim, C. B. (2003) *Biopolymers* **69,** 283–292.
22. Zamoon, J., Mascioni, A., Thomas, D. D. & Veglia, G. (2003) *Biophys. J.* **85,** 2589–2598.
23. Karim, C. B., Marquardt, C. G., Stamm, J. D., Barany, G. & Thomas, D. D. (2000) *Biochemistry* **39,** 10892–10897.
24. Kimura, Y., Kurzydlowski, K., Tada, M. & MacLennan, D. H. (1996) *J. Biol. Chem.* **271,** 21726–21731.
25. Kimura, Y., Asahi, M., Kurzydlowski, K., Tada, M. & MacLennan, D. H. (1998) *FEBS Lett.* **425,** 509–512.
26. MacLennan, D. H. & Toyofuku, T. (1996) *Soc. Gen. Physiol. Ser.* **51,** 89–103.
27. Toyoshima, C., Nakasako, M., Nomura, H. & Ogawa, H. (2000) *Nature* **405,** 647–655.
28. Toyoshima, C. & Nomura, H. (2002) *Nature* **418,** 605–611.
29. Lamberth, S., Schmid, H., Muenchbach, M., Vorherr, T., Krebs, J., Carafoli, E. & Griesinger, C. (2000) *Helv. Chim. Acta* **83,** 2141–2152.
30. Pollesello, P., Annila, A. & Ovaska, M. (1999) *Biophys. J.* **76,** 1784–1795.
31. Chen, B. & Bigelow, D. J. (2002) *Biochemistry* **41,** 13965–13972.
32. Hubbell, W. L., Cafiso, D. S. & Altenbach, C. (2000) *Nat. Struct. Biol* **7,** 735–739.
33. Toniolo, C., Valente, E., Formaggio, F., Crisma, M., Pilloni, G., Corvaja, C., Toffoletti, A., Martinez, G. V., Hanson, M. P., Millhauser, G. L., *et al*. (1995) *J. Pept. Sci.* **1,** 45–57.
34. Monaco, V., Formaggio, F., Crisma, M., Toniolo, C., Hanson, P. & Millhauser, G. L. (1999) *Biopolymers* **50,** 239–253.
35. Monaco, V., Formaggio, F., Crisma, M., Toniolo, C., Hanson, P., Millhauser, G., George, C., Deschamps, J. R. & Flippen-Anderson, J. L. (1999) *Bioorg. Med. Chem.* **7,** 119–131.
36. Karim, C. B., Paterlini, M. G., Reddy, L. G., Hunter, G. W., Barany, G. & Thomas, D. D. (2001) *J. Biol. Chem.* **276,** 38814–38819.
37. Marchetto, R., Schreier, S. & Nakaie, C.R. (1993) *J. Am. Chem. Soc.* **115,** 11042–11043.
38. Formaggio, F., Bonchio, M., Crisma, M., Peggion, C., Mezzato, S., Polese, A., Barazza, A., Antonello, S., Maran, F., Broxterman, Q. B., *et al*. (2002) *Chemistry* **8,** 84–93.
39. Martin, L., Ivancich, A., Vita, C., Formaggio, F. & Toniolo, C. (2001) *Peptide Res.* **58,** 424–432.
40. Nakaie, C. R., Schreier, S. & Paiva, A. C. (1983) *Biochim. Biophys. Acta* **742,** 63–71.
41. Reddy, L. G., Cornea, R. L., Winters, D. L., McKenna, E. & Thomas, D. D. (2003) *Biochemistry* **42,** 4585–4592.
42. Reddy, L. G., Autry, J. M., Jones, L. R. & Thomas, D. D. (1999) *J. Biol. Chem.* **274,** 7649–7655.
43. Kirby, T. L., Karim, C. B. & Thomas, D. D. (2004) *Biochemistry* **43,** 5842–5852.
44. Budil, D. E., Lee, S., Saxena, S. & Freed, J. H. (1996) *J. Magn. Reson.* **120,** 155–189.
45. Gross, A. & Hubbell, W. L. (2002) *Biochemistry* **41,** 1123–1128.
46. Altenbach, C., Greenhalgh, D. A., Khorana, H. G. & Hubbell, W. L. (1994) *Proc. Natl. Acad. Sci. USA* **91,** 1667–1671.
47. McNulty, J. C., Thompson, D. A., Carrasco, M. R. & Millhauser, G. L. (2002) *FEBS Lett.* **529,** 243–248.
48. Bui, T. T., Formaggio, F., Crisma, M., Monaco, V., Toniolo, C., Hussain, R. & Siligardi, G. (2000) *J. Chem. Soc. Perkin Trans. 2*, 1043–1046.
49. Hanson, P., Anderson, D. J., Martinez, G. V., Millhauser, G. L., Formaggio, F., Crisma, M., Toniolo, C. & Vita, C. (1998) *Mol. Phys.* **95,** 957–966.
50. Friedrich, C., Scott, M. G., Karunaratne, N., Yan, H. & Hancock, R. E. (1999) *Antimicrob. Agents Chemother.* **43,** 1542–1548.
51. Victor, K. G. & Cafiso, D. S. (2001) *Biophys. J.* **81,** 2241–2250.
52. Metcalfe, E., Zamoon, J., Thomas, D. D. & Veglia, G. (2004) *Biophys. J.* **87,** 1205–1214.
53. Columbus, L. & Hubbell, W. L. (2002) *Trends Biochem. Sci.* **27,** 288–295.